OPEN ACCESS Freely available online

PLoS GENETICS

Mapping of the Disease Locus and Identification of *ADAMTS10* As a Candidate Gene in a Canine Model of Primary Open Angle Glaucoma

John Kuchtey[1,2], Lana M. Olson[3], Tommy Rinkoski[4¤], Edward O. MacKay[4], T. M. Iverson[2,5], Kirk N. Gelatt[4], Jonathan L. Haines[2,3], Rachel W. Kuchtey[1,2,3]*

1 Vanderbilt Eye Institute, Vanderbilt University Medical Center, Nashville, Tennessee, United States of America, **2** Vanderbilt Vision Research Center, Vanderbilt University, Nashville, Tennessee, United States of America, **3** Center for Human Genetics Research, Vanderbilt University Medical Center, Nashville, Tennessee, United States of America, **4** Department of Small Animal Clinical Sciences, College of Veterinary Medicine, University of Florida, Gainesville, Florida, United States of America, **5** Departments of Pharmacology and Biochemistry, Vanderbilt University Medical Center, Nashville, Tennessee, United States of America

Abstract

Primary open angle glaucoma (POAG) is a leading cause of blindness worldwide, with elevated intraocular pressure as an important risk factor. Increased resistance to outflow of aqueous humor through the trabecular meshwork causes elevated intraocular pressure, but the specific mechanisms are unknown. In this study, we used genome-wide SNP arrays to map the disease gene in a colony of Beagle dogs with inherited POAG to within a single 4 Mb locus on canine chromosome 20. The Beagle POAG locus is syntenic to a previously mapped human quantitative trait locus for intraocular pressure on human chromosome 19. Sequence capture and next-generation sequencing of the entire canine POAG locus revealed a total of 2,692 SNPs segregating with disease. Of the disease-segregating SNPs, 54 were within exons, 8 of which result in amino acid substitutions. The strongest candidate variant causes a glycine to arginine substitution in a highly conserved region of the metalloproteinase ADAMTS10. Western blotting revealed ADAMTS10 protein is preferentially expressed in the trabecular meshwork, supporting an effect of the variant specific to aqueous humor outflow. The Gly661Arg variant in ADAMTS10 found in the POAG Beagles suggests that altered processing of extracellular matrix and/or defects in microfibril structure or function may be involved in raising intraocular pressure, offering specific biochemical targets for future research and treatment strategies.

Citation: Kuchtey J, Olson LM, Rinkoski T, MacKay EO, Iverson TM, et al. (2011) Mapping of the Disease Locus and Identification of *ADAMTS10* As a Candidate Gene in a Canine Model of Primary Open Angle Glaucoma. PLoS Genet 7(2): e1001306. doi:10.1371/journal.pgen.1001306

Editor: Gregory S. Barsh, Stanford University, United States of America

Received June 1, 2010; **Accepted** January 12, 2011; **Published** February 17, 2011

Funding: This work was supported by an Unrestricted Challenge Grant (Vanderbilt Eye Institute) and Career Development Award (RWK) from Research to Prevent Blindness, David K. Wilson Discovery Grant (RWK), MAPS Grant from the American Glaucoma Foundation (RWK), Vanderbilt Eye Institute Chairman's Discovery Grant (RWK, JK), NIH grant R01EY020894 (RWK), NIH grant EY018435 (TMI), and National Eye Institute Grant P30-EY008126 (Core Grant in Vision Research). The funders had no role in study design, data collection and analysis, decision to publish, or preparation of the manuscript.

Competing Interests: The authors have declared that no competing interests exist.

* E-mail: rachel.kuchtey@vanderbilt.edu

¤ Current address: Mayo Clinic, Department of Molecular Medicine, Rochester, Minnesota, United States of America

Introduction

Elevated intraocular pressure is a strong risk factor for glaucoma development and progression [1]. In POAG, increased resistance to outflow of aqueous humor through the trabecular meshwork is the cause of elevated intraocular pressure [2]. Currently, the only proven treatments for POAG patients involve reduction of intraocular pressure by inhibiting aqueous humor production, or bypassing the diseased trabecular meshwork. The mechanisms of increased resistance to aqueous humor outflow are not well-understood [2], but may involve changes in extracellular matrix composition of the trabecular meshwork [3].

Linkage studies have identified a number of POAG loci [4]. So far only three genes have been shown to be associated with POAG [4], but they account for only a small fraction of POAG cases, and none have shed much light on the disease process. Although genome-wide association studies could be a powerful tool to establish more POAG loci, this requires recruitment of a large number of patients. Moreover, causal association between sequence variants and disease can be difficult to establish in human studies. In this study, we have used a canine model to identify a candidate POAG gene, which has the advantage of availability of tissues from normal and affected dogs as well as future gene rescue experiments to investigate the pathogenic mechanisms of the gene variant.

A colony of Beagle dogs established in 1972 [5], which is a well-characterized and naturally occurring animal model of POAG, was used for this study. For POAG-affected dogs in this colony, increases in intraocular pressure begin at 8 to 16 months of age, due to increased resistance to outflow of aqueous humor [6], despite normal appearing open iridocorneal angles. As with POAG in humans, optic nerve cupping, loss of optic nerve axons [7] and vision loss occur in affected Beagles following slowly progressing and sustained elevations of intraocular pressure, if left untreated. Multigenerational breeding experiments have shown that POAG in the Beagle colony is inherited as an autosomal recessive trait [8].

Domestication of the dog from wolves and recent breed creations have resulted in extensive linkage disequilibrium and

Author Summary

Primary open angle glaucoma (POAG) is a leading cause of vision loss and blindness affecting tens of millions of people. Ocular hypertension is a strong risk factor for the disease and the only effective target of treatment. Ocular hypertension results from increased resistance to outflow of aqueous humor through the trabecular meshwork, a specialized filtration tissue consisting of alternating layers of cells and connective tissue, but the specific reasons for the increased resistance are not known. The animal model for human POAG used in this study was a colony of Beagle dogs that carry an inherited form of the disease in which ocular hypertension is the primary manifestation. We have found a variant in *ADAMTS10* that belongs to a family of genes that contribute to formation of extracellular matrix and may itself be involved in formation of elastic microfiber structures. We found that the ADAMTS10 protein is expressed at particularly high levels in the trabecular meshwork. The candidate variant in *ADAMTS10* found in the POAG–affected Beagles suggests that altered processing of connective tissue and/or elastic microfiber defects may be involved in raising eye pressure, offering specific biochemical targets for future research and treatment strategies.

large haplotype blocks, which makes mapping Mendelian traits possible with far fewer markers and fewer individuals as needed for human studies [9,10]. The dog genome has been sequenced and microarrays for whole-genome high-density SNP genotyping have been established and used to map traits in dogs [10–12]. The aim of this study was to map the disease locus and then to identify candidate disease genes by high-throughput sequencing of the entire disease locus.

Results

To map the POAG locus, we genotyped 19 affected and 10 carrier dogs from the POAG Beagle colony using version 2 of the Affymetrix Canine Genome SNP array. Since the colony has been maintained primarily by affected to affected breeding, with periodic introduction of unrelated normal Beagles (Figure 1), we hypothesized that the disease allele would be contained within an extensive haplotype block homozygous for affected and heterozygous for carrier dogs. Therefore, we identified SNPs that fulfilled the zygosity criterion, defined as being both homozygous for all affected dogs and heterozygous for all carriers. Regions of homozygosity for all affected dogs were common for all chromosomes, as expected for the highly inbred pedigree. However, only Chromosome 20 contained SNPs heterozygous for all carriers (Figure 2A), consisting of 41 consecutive SNPs covering 4.7 Mb. Of those 41 SNPs, 27 consecutive SNPs were also homozygous for all affected dogs, satisfying the zygosity criterion (Figure 2B and Figure S1). Haplotype analysis of the region revealed informative recombination events within the pedigree that defined a 4 Mb locus in which all carriers were heterozygous and all affected dogs homozygous for the affected haplotype (Figure 2C).

In addition to applying the zygosity criterion, two-point and multipoint parametric linkage analyses of the pedigree genotype data were performed. Initial power calculations predicted that with the available pedigree, a single locus could be identified with a LOD score of 2.67. With genome-wide two-point analysis, regions with LOD score >2 were found on chromosomes 5, 15 and 20 (Figure 3A). Follow-up multipoint linkage analysis reduced the LOD score of the chromosome 5 region to below 0.5, excluding this as a candidate locus (Figure 3B). For chromosome 15, multipoint analysis did not reduce the LOD score (Figure 3C). However, haplotype analysis revealed a pattern of inheritance discordant with phenotype (Figure 4), excluding chromosome 15. The distal end of chromosome 20 had a two-point LOD score of 2.42 and a multipoint LOD score of 2.70 (Figure 3D), consistent with initial power calculations. This region identified by linkage analysis coincided with the 4 Mb locus identified by the zygosity criterion. Therefore, the results of genome-wide linkage analysis independently verified that the disease locus in the POAG Beagles maps to the same 4 Mb region of chromosome 20 identified using the zygosity criterion.

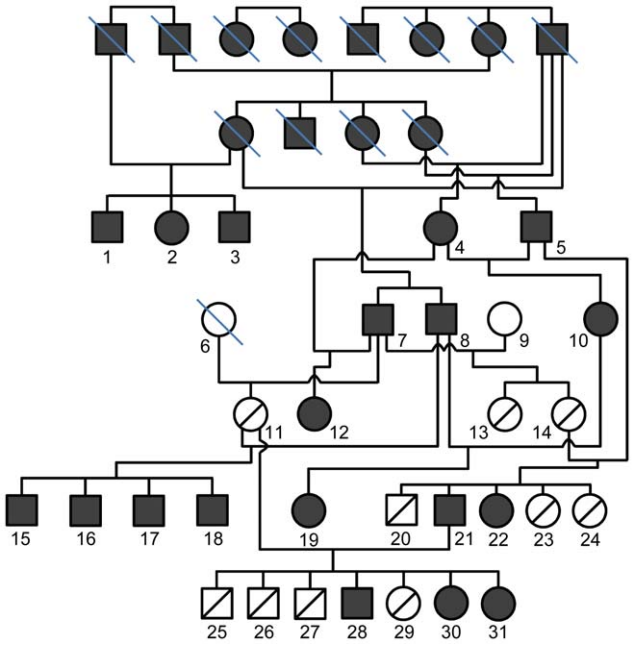

Figure 1. Pedigree of the POAG Beagle colony. The most recent generations of Beagles are shown, including the 30 dogs used for SNP genotyping (dogs 1–31, except dog 6). Prior to introduction of two unrelated normal Beagles (dogs 6 and 9), the colony had been maintained by mating affected to affected dogs for 5 generations, 3 of which are shown. Boxes: males, circles: females, filled symbols: POAG-affected, open symbols: not affected, open symbols with line from upper right to lower left: carriers, blue slash: sample not available.
doi:10.1371/journal.pgen.1001306.g001

Comparison of the 4 Mb POAG locus in dog with the human genome revealed shared synteny within a segment of human chromosome 19, previously identified as a quantitative trait locus for intraocular pressure in humans [13] (Figure 5A). The order and number of genes within the POAG locus on the canine chromosome are highly conserved in the human syntenic region (Figure 5B). Since increased intraocular pressure is the initial manifestation of disease in the POAG Beagles, synteny with the human intraocular pressure locus offers compelling biological support that the 4 Mb region contains the disease-causing genetic variant.

To identify the disease gene, the entire 4 Mb POAG locus in an affected and a carrier dog, as well as a normal dog from the colony (dogs 3, 9 and 11, Figure 1) was isolated by microarray-based sequence capture and then sequenced with the Illumina Genome Analyzer. Alignment of the sequences to the reference canine genome revealed 2,692 sequence variants segregating with disease

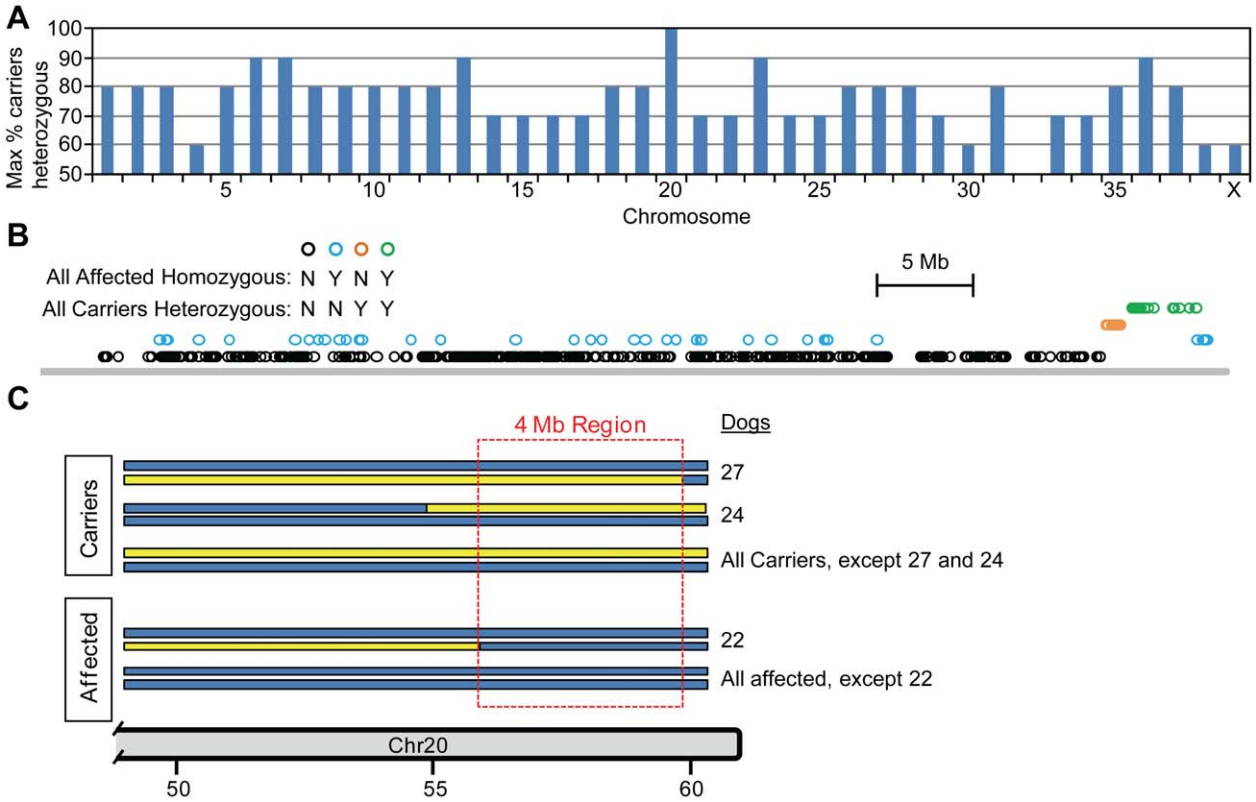

Figure 2. Mapping the POAG locus using the zygosity criterion. Genome-wide SNP data was evaluated to identify SNPs that satisfy the zygosity criterion, defined as being homozygous for all 19 POAG-affected dogs and heterozygous for all 10 carrier dogs. Calculating the percentage of carrier dogs heterozygous for each SNP revealed that only chromosome 20 contained SNPs for which all carriers (100%) were heterozygous (A). Within chromosome 20, the SNPs heterozygous for all carriers (orange and green symbols) form a contiguous block of 41 SNPs, within which 27 contiguous SNPs satisfy the zygosity criterion (green symbols) (B). Haplotype analysis revealed informative recombinations within the pedigree that defined a 4 Mb disease locus corresponding to the 27 SNPs satisfying the zygosity criterion (C). The location and genotypes of the SNPs satisfying the zygosity criterion are shown in Figure S1.
doi:10.1371/journal.pgen.1001306.g002

(homozygous for the affected dog and heterozygous for the carrier dog, with the additional criterion that the normal dog is not homozygous for the same allele as the affected dog). Of the segregating variants, 54 were located within coding regions of canine genes identified by the human protein alignment track of the UCSC genome browser (http://genome.ucsc.edu). Of the 54 variants within coding regions, 8 resulted in non-synonymous amino acid substitutions in 7 genes. Among those 8 variants, based on BLOSUM62 score for amino acid substitution and mammalian conservation score from the vertebrate multiz alignment and conservation track of the UCSC human genome browser, the best candidate variant was at position 56,097,365 of chromosome 20 (canFam build 2) from a G in the reference sequence, to an A in the affected dog. This variant was confirmed by conventional Sanger sequencing of affected, carrier and normal dogs from the POAG colony (Figure 6A). To determine the frequency of the disease allele (56097365 A) in the normal Beagle population, 48 Beagles not affected by glaucoma and not related to the colony were sequenced. Only one of the unaffected dogs was found heterozygous for the disease allele, the rest were homozygous for the normal allele, suggesting a disease allele frequency of ~1% in Beagles.

The 56097365 G->A variant is within exon 17 of *ADAMTS10*, a member of the disintegrin and metalloproteinase with thrombospondin motifs family of secreted proteases involved in formation of the extracellular matrix [14–16]. The variant results in a Gly->Arg substitution at position 661 within the protein sequence (NCBI accession XP_854320). The glycine at position 661 is completely conserved in 38 vertebrate species (7 representative species shown, Figure 6B). The Gly661Arg substitution was predicted to have a deleterious effect on protein function by the prediction programs SIFT [17] and SNPs3D [18] and occurs within the cysteine-rich domain (Figure 6C), which may be involved in regulation of protease activity [19].

Western blot analysis of protein extracts from tissues dissected from normal dog eyes showed high expression of ADAMTS10 protein in the trabecular meshwork, relative to other eye tissues examined (Figure 7). ADAMTS10 was also expressed in the cornea, and to a much less extent in the iris, ciliary body and optic nerve (Figure 7).

Structural modeling was performed using crystal structure of ADAMTS13 [20] to predict the structures of normal and Gly661Arg ADAMTS10 proteins. In the predicted fold of ADAMTS10, Gly661 is located within a tight turn (Figure 8A), suggesting a glycine may be required at this position for proper folding. Gly661 is predicted to be buried in the structure within the interface between the C_A and T_1 domains (Figure 8B). Substitution of arginine for glycine at position 661 would be sterically unfavorable, with the longer charged side chain of arginine extending into the T_1 domain (Figure 8C), suggesting that the Gly661Arg change would likely disrupt normal ADAMTS10 structure.

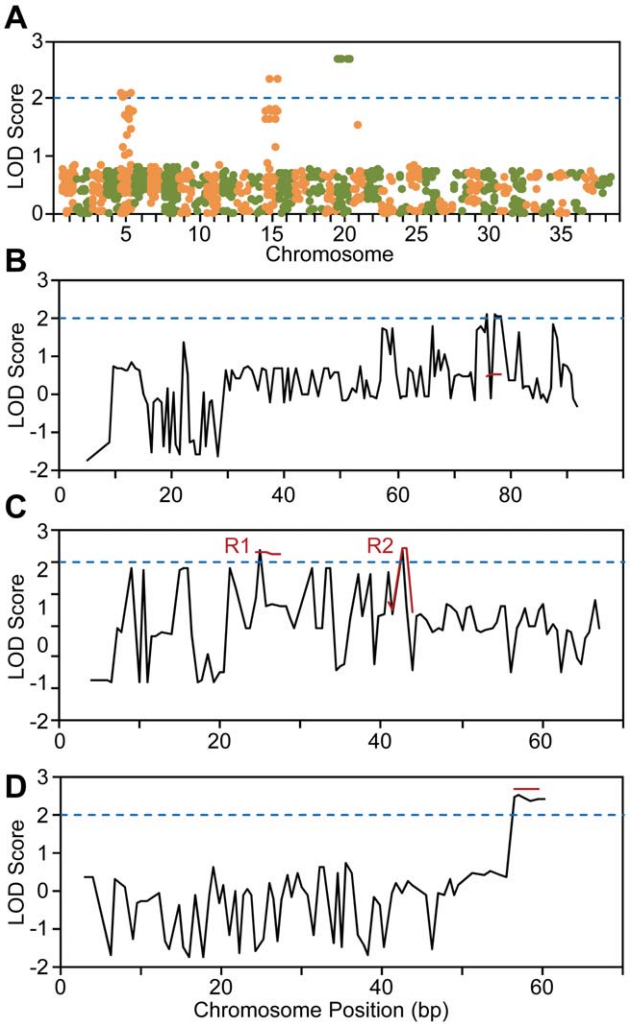

Figure 3. Genome-wide linkage analysis of SNP genotyping data. Calculation of two-point LOD scores revealed regions of interest, defined as having LOD score >2, on chromosomes 5, 15 and 20 (A). Two-point (black lines) and follow-up multipoint (red lines) linkage analyses are shown for chromosomes 5, 15 and 20 (B–D). Multipoint linkage analysis reduced the LOD score of the chromosome 5 region of interest to below 1 (B). Multipoint LOD scores for the two regions of interest (R1 and R2) of chromosome 15 were similar or higher than the two-point scores (C). The region on the distal end of chromosome 20 with two-point LOD score >2 had multipoint score of 2.70, and corresponds to the 4 Mb locus identified by the zygosity criterion.
doi:10.1371/journal.pgen.1001306.g003

To investigate possible effects of the Gly661Arg substitution on ADAMTS10 protein stability, the protein half-lives for normal and mutated ADAMTS10 were determined. Since ADAMTS10 produced by trabecular meshwork cells would be secreted into aqueous humor, half-lives were determined in the presence of aqueous humor. *In vitro* transcribed normal and mutated ADAMTS10 protein labeled with biotinylated lysine was incubated in aqueous humor for various time periods and the amount of ADAMTS10 remaining at each time point was determined by Western blotting with fluorescently labeled streptavidin. The Gly661Arg mutant appeared to decay more rapidly than did normal ADAMTS10 (Figure 9). The Log_2 of the band intensities were plotted *vs.* time to determine the protein half life, which is equal to the negative inverse of the slope of the best fit line. In each of four independent experiments, mutated ADAMTS10 decayed more rapidly than did normal ADAMTS10 (261+/−29.5 *vs.* 601+/−219.7 min., mean +/− SD, half-lives for mutated and normal, respectively, significantly different, $p<0.05$). The slopes of the lines fit to data from all four experiments, combined by normalizing band intensities to the initial time point, were significantly different ($p<0.001$) and correspond to half lives of 255.8 min. for mutated and 636.9 min. for normal ADAMTS10 (Figure 9C). These results suggest that mutated ADAMTS10 decays more rapidly, with a protein half-life ~40% that of normal.

Discussion

By application of the zygosity criterion, linkage and haplotype analyses, we were able to map the Beagle POAG locus to a single 4 Mb region on chromosome 20. This canine POAG locus is syntenic with a region on human chromosome 19 within a quantitative trait locus for regulation of intraocular pressure identified by a genome-wide scan of 486 families [13]. Since ocular hypertension occurs early in the disease process in the Beagles, synteny with the intraocular pressure locus gives biological support to the genetic identification of the POAG locus and suggests that the disease gene directly participates in intraocular pressure regulation. Furthermore, synteny with the human locus suggests that the disease gene found in the Beagles may also be disrupted in human glaucoma patients.

Using affected and unaffected dogs of other breeds to fine map the disease locus has proven to be an effective approach in other canine genetic studies [10]. However, because clinical identification of POAG cases in dogs is rare, this approach would be challenging and further would require the assumption that the POAG locus in Beagles is shared with affected dogs of other breeds. Alternatively, refining the locus by further breeding within the colony to allow for informative recombinations would be time consuming and costly since definitive diagnosis cannot be made until two years of age.

To overcome these limitations, we obtained high quality sequence information for the entire 4 Mb locus by sequence capture and next-generation sequencing. Using this approach, 2,692 single nucleotide variants that segregated with disease were identified, 54 of which were within exons, 8 of which were nonsynonomous. Since POAG in the POAG Beagle colony is autosomal recessive with 100% penetrance, we focused on nonsynonomous changes because these are likely to have strong functional effects. However, synonomous changes in coding regions or variants outside coding regions could have pathogenic effects and cannot be ruled out. In addition, our sequence capture and sequence analysis rely on the quality of the reference canine genome and therefore our approach could miss variants due to errors in the reference genome assembly or annotation.

Among the 8 nonsynonomous variants segregating with disease, the strongest candidate identified was a single base pair change in the affected dogs that results in a non-conservative amino acid substitution in a region of ADAMTS10 that is highly conserved in vertebrate species. In POAG-affected dogs, an arginine is substituted for a glycine at amino acid position 661 which is an invariant amino acid in ADAMTS10 in 38 species, from lamprey to human. Consistent with a highly penetrant rare disease allele, the frequency of the variant in *ADAMTS10* estimated from genotyping 48 unrelated normal Beagles was 1%.

ADAMTS10 is a member of a family of secreted metalloproteinases [14,16]. All ADAMTS family members share a common structural organization including a metalloproteinase domain followed by a disintegrin-like module, a thrombospondin repeat unit, a cysteine-rich domain and a spacer region (see Figure 6C).

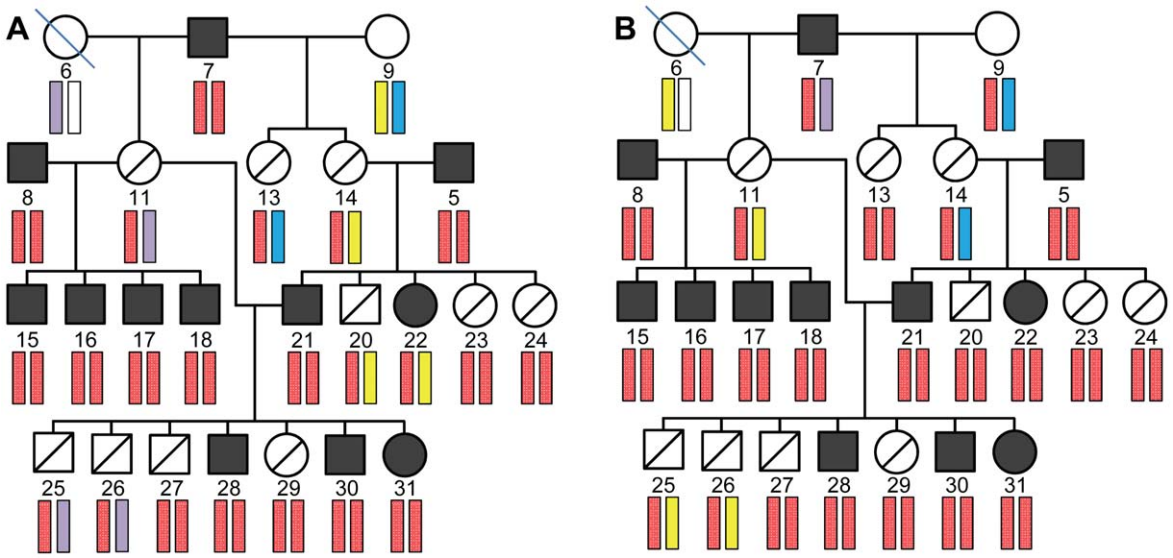

Figure 4. Haplotype analysis of chromosome 15 regions R1 and R2. Although region R1 (A) and R2 (B) had multipoint LOD scores >2, as shown in Figure 3C, their inheritance patterns were discordant with disease status, ruling out these regions as containing the disease allele. The minimal informative pedigree is shown, with dog numbers and symbols corresponding to the pedigree shown in Figure 1. The chromosomal positions for the SNPs defining the haplotypes are shown in Figure S2.
doi:10.1371/journal.pgen.1001306.g004

Diversity within the ADAMTS family largely arises from structural differences in ancillary domains of the carboxy-terminal half of the proteins. The Gly661Arg variant found in this study is within the cysteine-rich domain of ADAMTS10 and is predicted to disrupt protein function by the amino acid substitution prediction programs SIFT [17] and SNPs3D [18]. Consistent with this, our homology modeling of the ADAMTS10 structure suggests that the Gly661 residue is located within a tight turn and is buried within the interface between the cysteine rich and thrombospondin repeat domains. The long polar side chain of arginine substituted at this position is predicted to disrupt the normal protein fold. Consistent with disruption of normal protein folding, we found that the Gly661Arg form of ADAMTS10 is less stable, with a protein half-life ~40% that of normal ADAMTS10. Although we cannot be certain if the reticulocyte lysate-based *in vitro* transcription and translation system produced normally folded protein, this system has been used to produce functional secreted proteins such as metalloproteinases [21], neutrophil elastase [22] and myocilin [23]. Any effects of the *in vitro* system on folding would be experienced by both the normal and mutated proteins in our assays. Our data show that the mutated form of ADAMTS10 has a shortened half-life, consistent with our homology modeling which suggested that the Gly661Arg substitution would disrupt interactions at the interface of two domains.

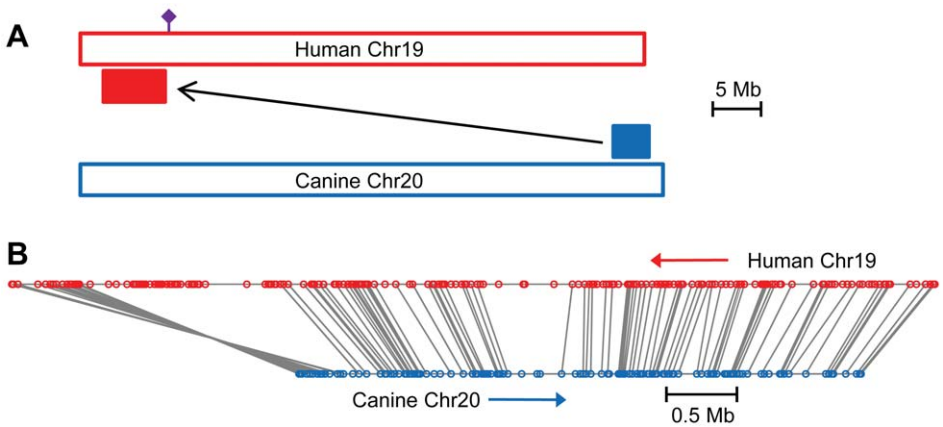

Figure 5. The canine POAG locus is syntenic with a human quantitative trait locus for intraocular pressure. The 4 Mb POAG locus (solid blue rectangle) found in the Beagle colony maps to a 6.5 Mb region (solid red rectangle) on the short arm of human chromosome 19, and within a 20 cM quantitative trait locus for intraocular pressure in humans located near microsatellite marker D19S586 (purple symbol) (A). The number and order of genes within the canine POAG locus and the syntenic region of human chromosome 19 are well conserved (B). Canine genes, blue circles, human genes, red circles. Orthologous genes are connected by gray lines. The canine chromosome 20 locus extends from base pair positions 55,881,144 to 59,844,869, corresponding to human chromosome 19 base pair positions 2,389,784 to 8,841,863. Direction of increasing base pair number of the reference sequence is indicated by red and blue arrows (B). At the centromeric end of the canine locus, a 0.3 Mb portion of the locus is inverted with respect to the human chromosome (B). The figure is drawn to scale, with scale bars of 5 Mb (A) and 0.5 Mb (B) shown.
doi:10.1371/journal.pgen.1001306.g005

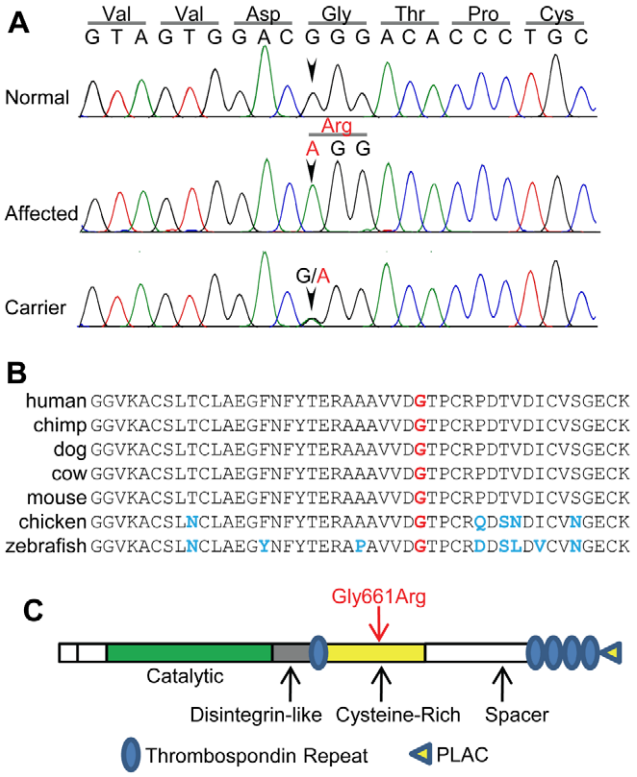

Figure 6. The 56097365 G->A variant is within a highly conserved region of *ADAMTS10*. The G->A variant identified by Illumina sequencing was confirmed by Sanger sequencing of normal, affected and carrier dogs from the POAG Beagle colony (A). The variant causes a glycine residue at amino acid position 661 (red) to be changed to an arginine within exon 17 of *ADAMTS10* (B). This glycine is conserved in the sequence of 38 vertebrate species (Human, Chimp, Gorilla, Orangutan, Rhesus Monkey, Baboon, Marmoset, Tarsier, Mouse lemur, Bushbaby, Mouse, Rat, Kangaroo rat, Guinea pig, Squirrel, Rabbit, Dolphin, Cow, Horse, Cat, Dog, Megabat, Hedgehog, Elephant, Tenrec, Armadilo, Wallaby, Opossum, Platypus, Chicken, Zebra finch, Xenopus tropicalis, Tetraodon, Fugu, Stickleback, Medaka, Zebra fish, and Lamprey), 7 of which are shown aligned (B). The Gly661Arg variant occurs within the cysteine-rich domain of ADAMTS10 (C).
doi:10.1371/journal.pgen.1001306.g006

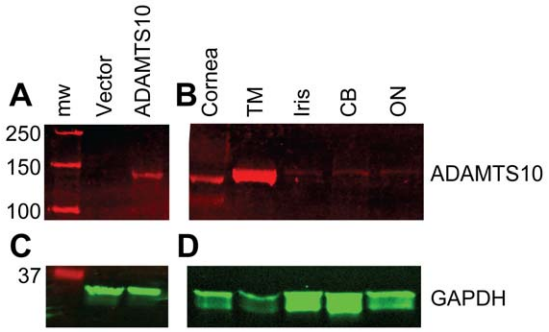

Figure 7. ADAMTS10 protein is highly expressed in the trabecular meshwork. Western blotting using an anti-ADAMTS10 (A and B) or anti-GAPDH (C and D) antibody was performed on cell lysates (A and C) or protein extracts from normal canine eye tissues (B and D). For cell lysates, 5 µg total protein from cells transfected with empty vector (Vector), or a vector containing an ADAMTS10 construct (ADAMTS10) were loaded in each lane (A and C). For eye tissue protein extracts, 10 µg total protein were loaded in each lane (B and D). TM: trabecular meshwork, CB: ciliary body, ON: optic nerve. Molecular weight marker (mw) is shown with molecular weights in kDa.
doi:10.1371/journal.pgen.1001306.g007

Clinical evidence for the importance of the cysteine rich domain in ADAMTS function comes from patients with thrombotic thrombocytopenic purpuria (OMIM #274150) who have auto-antibodies recognizing the cysteine-rich domain of ADAMTS13, causing reduced proteolytic activity of ADAMTS13 *in vivo* and *in vitro* [24,25]. Structural studies and deletion analysis have established that the cysteine-rich domain plays a vital role in regulation of protease activity or substrate recognition for ADAMTS family proteins [20,25]. In addition, alignment of the cysteine-rich domains of all 19 human ADAMTS family members and 5 related ADAMTSL proteins by Akiyama *et al.* [20], revealed that Gly661 of ADAMTS10 is an invariant amino acid. Such stringent evolutionary conservation of this glycine residue, across 38 vertebrate species and within 24 protein superfamily members, supports the hypothesis that the arginine substitution would have a detrimental effect on ADAMTS10 function.

Unlike the three POAG genes identified thus far in humans (*MYOC*, *WDR36* and *OPTN*) [4], the *ADAMTS10* variant identified in this study has obvious functional implications, supporting *ADAMTS10* as a strong candidate gene. A role for metalloproteinases in ocular hypertension has long been suggested by numerous *in vitro* studies [26]. Changes in the amount or composition of extracellular matrix within the trabecular meshwork have been hypothesized to contribute to ocular hypertension by increasing resistance to outflow of aqueous humor through the trabecular meshwork [3]. Although the specific substrate for ADAMTS10 is unknown, other ADAMTS family members are known to participate in collagen processing and proteoglycan degradation. ADAMTS10 is likely to function in some capacity in regulation of extracellular matrix and therefore disruption of its function could lead to POAG by increasing resistance to aqueous humor outflow through the trabecular meshwork. Several ADAMTS family members have been investigated as candidates for regulating outflow resistance, and it has been shown that perfusion of anterior segment organ cultures with ADAMTS4 increases outflow facility [27]. The faster decay of the Gly661Arg ADAMTS10 would likely reduce the amount of ADAMTS10 available, which could possibly result in increased resistance to aqueous humor outflow. Future studies with anterior segment organ cultures perfused with normal and mutated ADAMTS10 could test this hypothesis.

The Beagles of the POAG colony are phenotypically normal with no systemic abnormalities other than POAG in the affected dogs. Our Western blotting results showed that ADAMTS10 is expressed at high levels within the trabecular meshwork as compared to other eye tissues, which would be consistent with an effect of the Gly661Arg *ADAMTS10* variant specific to aqueous humor outflow.

Mutations in *ADAMTS10* have been identified in human patients with autosomal recessive Weill-Marchesani syndrome (WMS) [28,29], a rare disease with systemic features including short stature and stubby hands and feet (OMIM #277600). A mutation in type I fibrillin has also been found in autosomal dominant WMS [30], which is clinically indistinguishable from the autosomal recessive form [31], suggesting a functional link between *ADAMTS10* and type I fibrillin. WMS belongs to a group of rare connective tissue disorders, including Marfan syndrome (OMIM #154700), for which causative mutations in type I fibrillin, a major constituent of microfibrils [32], have been found. While glaucoma is common in WMS patients [31], the mechanism is not well-studied, due to the extremely small patient population. The prevalence of glaucoma in Marfan syndrome patients is higher than in the general population [33]. Clinically,

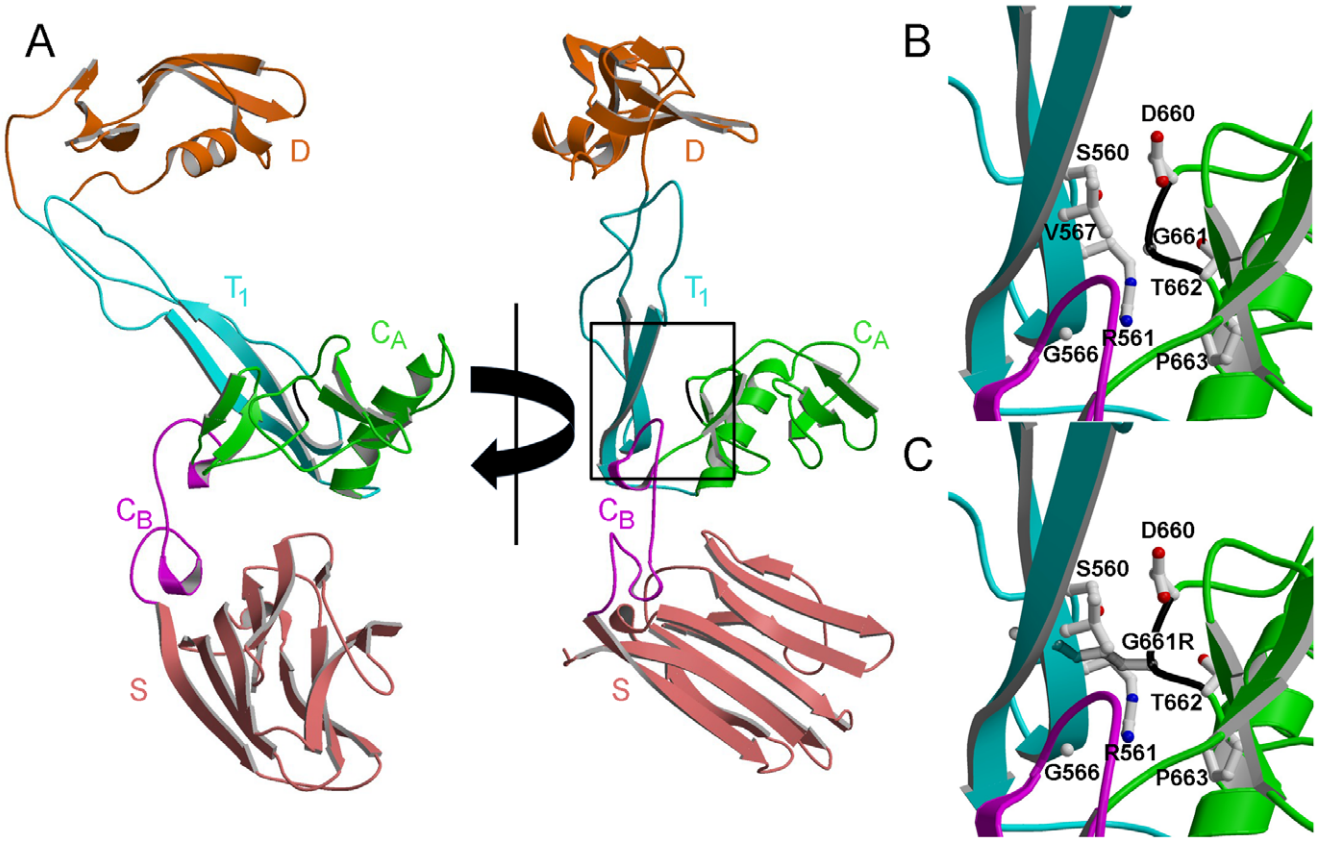

Figure 8. Structural modeling predicts disruption of the normal protein fold by the Gly661Arg variant of ADAMTS10. The structure of normal (A and B) and Gly661Arg mutated (C) ADAMTS10 was predicted by homology modeling using the amino acid sequence of ADAMTS10 and the crystal structure of ADAMTS13 [20], which includes the disintegrin-like domain (D), the thrombospondin-1 type-1 repeat domain (T_1), the amino-terminal portion of the cysteine-rich domain (C_A), the carboxy-terminal portion of the cysteine-rich domain (C_B) and the spacer domain (S). Rotated views (90°) of the entire predicted structure for ADAMTS10 are shown, with the portion of backbone corresponding to Gly661 in the C_A domain colored black (A). The boxed portion in A is expanded to show the substitution site for normal (B) and mutated (C) ADAMTS10, with selected amino acid side chains shown.
doi:10.1371/journal.pgen.1001306.g008

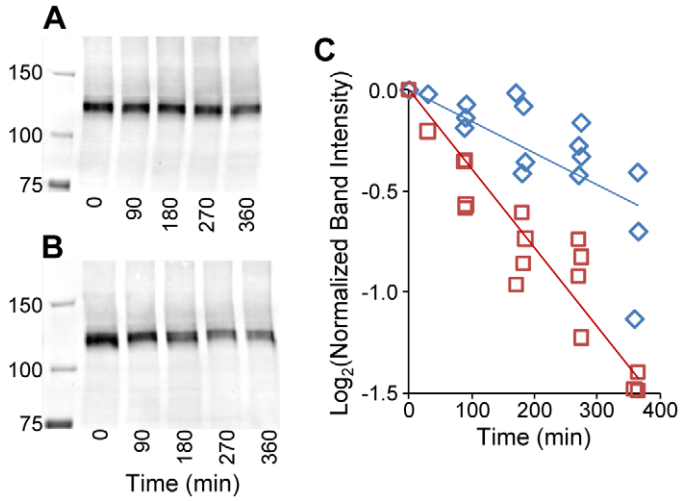

Figure 9. Gly661Arg-mutated ADAMTS10 decays more rapidly than does normal ADAMTS10. *In vitro* transcribed normal (A and blue diamonds in C) and Gly661Arg mutated (B and red squares in C) ADAMTS10 labeled with biotinylated lysine residues was incubated in aqueous humor for various times at 37°C. A band of ~130 kDa was detected by Western blotting with fluorescently labeled streptavidin, as shown in a representative experiment for both normal (A) and mutated (B) ADAMTS10 (incubation times, in minutes, shown below lanes). The slopes of the lines fit to data from all four experiments combined by normalizing band intensities to the initial time point (C) were significantly different ($p<0.001$) and correspond to half lives of 255.8 min. for mutated (red squares and red line) and 636.9 min. for normal ADAMTS10 (blue diamonds and blue line) (C). Molecular weight markers are shown in the left-most lanes of the blots (A and B) with mw in kDa indicated.
doi:10.1371/journal.pgen.1001306.g009

glaucoma in Marfan syndrome most often presents as POAG, with elevated intraocular pressure and open iridocorneal angles [33]. As type I fibrillin is involved in microfibril formation and function, presentation of POAG in patients with Marfan syndrome caused by type I fibrillin mutations suggests that microfibril defects may be involved in POAG pathogenesis. This notion is supported by another common ocular manifestation in WMS and Marfan syndrome, ectopia lentis (dislocated or malpositioned lens). Consistent with a defect in microfibril structure or function, ectopia lentis is caused by defects in the zonule fibers that hold the lens in place and are composed of fibrillin-containing microfibrils [34]. Recently, mutations were found in other members of the ADAMTS superfamily, *ADAMTS17* in autosomal recessive WMS [29] and *ADAMTSL4* in isolated ectopia lentis [35], supporting a role for ADAMTS family members in microfibril structure and function.

Ultrastructural studies of human trabecular meshwork have shown changes with age that are more pronounced in POAG patients, including a thickening of sheaths that surround elastin fibers and are composed of extracellular matrix, including fibrillin and fine fibrils, as well as an accumulation of sheath-derived plagues in the aqueous humor outflow pathway [36]. We have previously described similar changes in the trabecular meshwork of POAG-affected Beagles [37], which could be explained by microfibril defects caused by the Gly661Arg variant in the *ADAMTS10* gene. Additionally, microfibrils play an important regulatory role in the homeostasis of extracellular matrix by controlling the activation and localization of TGFβ [32], which is elevated in the aqueous humor of glaucomatous eyes [38,39]. Involvement of microfibril defects in glaucoma is further suggested by recent findings in primary congenital glaucoma of a null mutation in LTBP2, which shares homology with fibrillins and is a structural and functional component of microfibrils [40]. Identification of the Gly661Arg variant of *ADAMTS10* in the POAG Beagles in this study provides genetic evidence that microfibril abnormalities may be involved in increased resistance to outflow of aqueous humor through the trabecular meshwork in POAG.

The precise mechanisms of increased resistance to outflow of aqueous humor have remained a long-standing puzzle in glaucoma research. Current treatments for POAG patients involve reduction of intraocular pressure by inhibiting production of aqueous humor, or bypassing the diseased outflow pathway, but do not address the root of the problem. The robust expression of ADAMTS10 in the trabecular meshwork suggests that any defect in ADAMTS10 function caused by the Gly661Arg variant could have particularly pronounced effects on the functioning of the trabecular meshwork, specifically affecting aqueous humor outflow. Identification of *ADAMTS10* as a candidate gene in the POAG Beagles suggests that altered processing of extracellular matrix and/or defects in microfibril structure or function may be involved in raising intraocular pressure, offering specific biochemical targets for future research and treatment strategies.

Materials and Methods

SNP genotyping

Blood samples from dogs were obtained by licensed veterinarians or veterinary technicians by standard venipuncture, in accordance with the Institutional Animal Care and Use Committees of Vanderbilt University and the University of Florida. A total of 48 canine DNA samples, including 30 dogs from the POAG Beagle colony, 7 unrelated normal Beagles and 11 unrelated mixed-breed dogs, were genotyped using version 2 of the Affymetrix genome-wide SNP genotyping array (http://www.broadinstitute.org/mammals/dog/caninearrayfaq.html). For combined genotype data of all dogs, 40,600 informative SNPs had call rates >90%, and were heterozygous for <50% of dogs. For duplicate samples, 99.6% of SNPs received identical calls. The disease status of dogs was determined by clinical eye exams by veterinary ophthalmologists. The minimal age of the dogs at final diagnosis was 2.2 years.

Linkage analysis

Initial power calculations were performed using the SIMLINK V 4.12 program (http://csg.sph.umich.edu/boehnke/simlink.php). Two-point and multipoint linkage analyses of the genome-wide SNP data were performed using SuperLink Online [41] assuming an autosomal recessive model with complete penetrance. Dogs 1 through 31, except dog 6, were included in the analysis (Figure 1). SNPs uninformative for Beagles were removed from analysis. Mendelian error checking was performed and inconsistent SNPs removed for all individuals. Minor allele frequencies were calculated using SNP data from 8 unaffected Beagles whose unrelatedness was confirmed using the Graphical Representation of Relationship (GRR) software package [42].

Microarray-based DNA capture

Enrichment for genomic sequence within the 4 Mb locus was carried out using capture microarrays designed and manufactured by Roche NimbleGen, using build 2 of the canine genome. The capture arrays consisted of 385,000 capture probes >60 bp in length, designed to capture all non-repetitive sequence from base position 55,800,000 to 59,850,000 on canine chromosome 20. Sequence capture was carried out on 3 dogs from the POAG Beagle colony (dogs 3, 9, and 11, Figure 1), essentially as described in Albert et al. [43] and Okou et al. [44], with modifications to optimize for the Illumina Genome Analyzer II sequencing platform.

Illumina sequencing

Hybridization of the captured DNA fragments to the flow cell and amplification to form clusters was performed using the Illumina cluster station, following the standard Illumina protocol. The captured DNA fragments were used at a final concentration of 5 pM during hybridization/cluster generation to achieve cluster density of ~160,000 clusters/tile. Paired end, 38 base pair read sequencing was carried out with the Illumina Genome Analyzer II. Fluorescent images were converted into base pair calls using the Illumina Pipeline software. Paired end alignments to the canine genome build 2 were carried out using Bowtie [45]. For the 3 samples, 53.7% of the reads aligned to the 4.05 Mb target region representing 0.17% of the genome, yielding a 316-fold enrichment of the target sequence. The percentage of the capture region covered >8-fold ranged from 91.3% to 92.1%. The average coverage of genes, represented by the human protein alignment track in the UCSC genome browser (http://genome.ucsc.edu/) ranged from 93.1% to 94.4%. For the 29 SNPs in the capture region represented on the SNP genotyping array, complete concordance in genotype calls was found between the Illumina sequencing and SNP array data. Bases different from the reference canine sequence (variant SNPs) were identified using SAMtools [46] (http://samtools.sourceforge.net). SNPs segregating with disease were defined as being a homozygous variant in the affected dog and heterozygous for the carrier dog, with the additional criterion that the normal dog could not be homozygous for the variant found in the affected dog. Segregation of the 56097365 G->A variant with disease status was confirmed by Sanger sequencing of affected, carrier and normal dogs from the POAG Beagle colony. To determine the disease allele frequency in

Beagles, 48 normal Beagles examined by licensed veterinarians and found to be not affected by glaucoma were also sequenced. The normal Beagles were unrelated to the POAG colony and did not share common grandparents.

Western blotting of eye tissue protein extracts

Postmortem eyes from dogs were obtained by veterinary technicians in accordance with the Institutional Animal Care and Use Committee of Vanderbilt University. Eyes were removed from normal dogs free of eye disease within 30 min after sacrifice. Cornea, trabecular meshwork, iris, ciliary body and optic nerve were isolated by dissection under a stereo microscope. Protein was extracted by homogenization in 150 mM LiCl, 50 mM Tris/ pH 7.5, 1 mM dithiothrietol, protease inhibitors and 1% lithium dodecyl sulfate. Protein concentration was determined using a fluorescence-based protein assay (Nano-Orange Protein Assay, Invitrogen). Lysates of HEK293 cells transiently transfected with either empty vector or vector containing an epitope-tagged, full length human *ADAMTS10* construct (Origene) were used as controls. For SDS-PAGE under reducing conditions, 10 µg of total protein from eye tissues or 5 µg from cell lysates were loaded into wells of 10% pre-cast polyacrylamide gels (Criterion, Bio-Rad). After SDS-PAGE, proteins were transferred to PVDF membrane (Bio-Rad). Standard Western blotting was performed using 1 µg/ml goat anti-human ADAMTS10 antibody (Santa Cruz) or 3.3 µg/ml mouse anti-human glyceraldehyde-3-phophate dehydrogenase (GAPDH) antibody (clone 6C5, Millipore). Blots were imaged and molecular weights determined using an Odyssey infrared imaging system (Li-Cor Biosciences). A single immunoreactive band for ADAMTS10 ran at an apparent mw of 130 kDa, the same as previously reported for the intact ADAMTS10 zymogen [15].

Homology modeling

The homology model of ADAMTS10 was calculated using the program I-TASSER [47] and is based on the structure of ADAMTS13 (PDB entry 3GHM; [20]). Superposition of the calculated model with ADAMTS13 in the program O [48] resulted in a RMS deviation of 1.0 Å for 347 C_α atoms. Figure 8 was made using MOLSCRIPT [49] and RASTER3D [50]. The domain nomenclature and color coding follow those of Akiyama *et al.* [20].

Protein half-life measurement

Canine aqueous humor was obtained from laboratory-quality dogs using protocols approved by the Institutional Animal Care and Use Committee of Vanderbilt University and placed immediately in sealed sterile tubes and stored at −80°C. An expression vector with a T7 promoter upstream of a cDNA insert encoding full-length human ADAMTS10 corresponding to NCBI accession number NM_030957 with a c-terminal Myc-DDK tag was obtained from Origene. The ADAMTS10 insert was verified by Sanger DNA sequencing on both strands. A PCR-based mutagenesis kit (Quick Change II, Stratagene) was used to introduce the G to A mutation found in the POAG-affected Beagles, resulting in a glycine to arginine substitution at amino acid 661 into the expression construct. Mutagenesis was confirmed by Sanger sequencing of the entire construct. A rabbit reticulocyte-based *in vitro* coupled transcription/translation kit (TNT Quick, Promega) was used to express normal and mutated ADAMTS10 protein from the expression vector constructs following the manufacturer's protocol. Modified lysine-specific tRNA was included in the reaction (Transcend tRNA, Promega) to produce ADAMTS10 protein with biotinylated lysines. To measure protein half-life, samples were made with 4 µl of *in vitro* reaction mixed with 26 µl aqueous humor in sterile O-ring-sealed tubes and placed in a 37°C water bath. At various times, samples were removed from the water bath and placed in −80°C. The aqueous humor used in the experiments was pooled from 3 individual dogs and included 50 µg/ml cycloheximide (Sigma) to prevent protein synthesis during incubation. Samples were separated by SDS-PAGE using 7.5% pre-cast polyacrylamide gels (Criterion, Bio-Rad). After SDS-PAGE, proteins were transferred to PVDF membrane (Bio-Rad). The membrane was blocked 1 h in PBS/1% casein and then probed with streptavidin conjugated to IRDye 680 (Li-Cor Biosciences). Membranes were imaged and molecular weights and background subtracted band intensities determined using an Odyssey infrared imaging system (Li-Cor Biosciences). A single band at the expected molecular weight of ~130 kDa was detected, similar to that reported previously [15] and found in eye tissue in this study. Protein decay was assumed to follow the equation:

$$A(t) = A(t=0) \times 2^{-t/h}$$

where A(t) is the amount of protein at time t, A(t = 0) is the amount of protein at time t = 0 and h is the half life. The decay equation can be rearranged to:

$$\mathrm{Log}_2[A(t)] = \mathrm{Log}_2[A(t=0)] - (1/h) \times t$$

By plotting the Log_2 of the band intensity versus time of incubation, the half-life of the protein was determined as the negative inverse of the slope of the linear fit to the data. Four independent experiments were performed.

Supporting Information

Figure S1 SNPs satisfying the zygosity criterion. The chromosome 20 base pair location and genotypes for all affected, all carrier as well as a normal unrelated Beagle introduced into the colony are shown.
Found at: doi:10.1371/journal.pgen.1001306.s001 (0.37 MB TIF)

Figure S2 Haplotypes for chromosome 15 regions of interest. The base pair locations and genotypes are shown for haplotypes representing region R1 (A) and R2 (B), with symbols used to represent the haplotypes shown below.
Found at: doi:10.1371/journal.pgen.1001306.s002 (0.43 MB TIF)

Acknowledgments

The authors thank Dr. Maria E. Källberg for helping to initiate this project and Caryn E. Plummer for clinical exams.

Author Contributions

Conceived and designed the experiments: JK RWK. Performed the experiments: JK TR EOM KNG RWK. Analyzed the data: JK LMO TMI JLH RWK. Contributed reagents/materials/analysis tools: JK LMO TR EOM TMI KNG JLH RWK. Wrote the paper: JK TMI RWK.

References

1. Kwon YH, Fingert JH, Kuehn MH, Alward WL (2009) Primary open-angle glaucoma. N Engl J Med 360: 1113–1124.
2. Johnson M (2006) 'What controls aqueous humour outflow resistance?'. Exp Eye Res 82: 545–557.

3. Acott TS, Kelley MJ (2008) Extracellular matrix in the trabecular meshwork. Exp Eye Res 86: 543–561.
4. Allingham RR, Liu Y, Rhee DJ (2009) The genetics of primary open-angle glaucoma: a review. Exp Eye Res 88: 837–844.
5. Gelatt KN, Peiffer RL, Jr., Gwin RM, Gum GG, Williams LW (1977) Clinical manifestations of inherited glaucoma in the beagle. Invest Ophthalmol Vis Sci 16: 1135–1142.
6. Peiffer RL, Jr., Gum GG, Grimson RC, Gelatt KN (1980) Aqueous humor outflow in beagles with inherited glaucoma: constant pressure perfusion. Am J Vet Res 41: 1808–1813.
7. Brooks DE, Strubbe DT, Kubilis PS, MacKay EO, Samuelson DA, et al. (1995) Histomorphometry of the optic nerves of normal dogs and dogs with hereditary glaucoma. Exp Eye Res 60: 71–89.
8. Gelatt KN, Gum GG (1981) Inheritance of primary glaucoma in the beagle. Am J Vet Res 42: 1691–1693.
9. Lindblad-Toh K, Wade CM, Mikkelsen TS, Karlsson EK, Jaffe DB, et al. (2005) Genome sequence, comparative analysis and haplotype structure of the domestic dog. Nature 438: 803–819.
10. Karlsson EK, Baranowska I, Wade CM, Salmon Hillbertz NH, Zody MC, et al. (2007) Efficient mapping of mendelian traits in dogs through genome-wide association. Nat Genet 39: 1321–1328.
11. Parker HG, VonHoldt BM, Quignon P, Margulies EH, Shao S, et al. (2009) An expressed fgf4 retrogene is associated with breed-defining chondrodysplasia in domestic dogs. Science 325: 995–998.
12. Drogemuller C, Karlsson EK, Hytonen MK, Perloski M, Dolf G, et al. (2008) A mutation in hairless dogs implicates FOXI3 in ectodermal development. Science 321: 1462.
13. Duggal P, Klein AP, Lee KE, Klein R, Klein BE, et al. (2007) Identification of novel genetic loci for intraocular pressure: a genomewide scan of the Beaver Dam Eye Study. Arch Ophthalmol 125: 74–79.
14. Porter S, Clark IM, Kevorkian L, Edwards DR (2005) The ADAMTS metalloproteinases. Biochem J 386: 15–27.
15. Somerville RP, Jungers KA, Apte SS (2004) Discovery and characterization of a novel, widely expressed metalloprotease, ADAMTS10, and its proteolytic activation. J Biol Chem 279: 51208–51217.
16. Apte SS (2009) A disintegrin-like and metalloprotease (reprolysin-type) with thrombospondin type 1 motif (ADAMTS) superfamily: functions and mechanisms. J Biol Chem 284: 31493–31497.
17. Kumar P, Henikoff S, Ng PC (2009) Predicting the effects of coding non-synonymous variants on protein function using the SIFT algorithm. Nat Protoc 4: 1073–1081.
18. Yue P, Melamud E, Moult J (2006) SNPs3D: candidate gene and SNP selection for association studies. BMC Bioinformatics 7: 166.
19. Smith KM, Gaultier A, Cousin H, Alfandari D, White JM, et al. (2002) The cysteine-rich domain regulates ADAM protease function in vivo. J Cell Biol 159: 893–902.
20. Akiyama M, Takeda S, Kokame K, Takagi J, Miyata T (2009) Crystal structures of the noncatalytic domains of ADAMTS13 reveal multiple discontinuous exosites for von Willebrand factor. Proc Natl Acad Sci U S A 106: 19274–19279.
21. Coulombe B, Skup D (1988) In vitro synthesis of the active tissue inhibitor of metalloproteinases encoded by a complementary DNA from virus-infected murine fibroblasts. J Biol Chem 263: 1439–1443.
22. Duan Z, Li FQ, Wechsler J, Meade-White K, Williams K, et al. (2004) A novel notch protein, N2N, targeted by neutrophil elastase and implicated in hereditary neutropenia. Mol Cell Biol 24: 58–70.
23. Fautsch MP, Johnson DH (2001) Characterization of myocilin-myocilin interactions. Invest Ophthalmol Vis Sci 42: 2324–2331.
24. Zheng XL, Wu HM, Shang D, Falls E, Skipwith CG, et al. Multiple domains of ADAMTS13 are targeted by autoantibodies against ADAMTS13 in patients with acquired idiopathic thrombotic thrombocytopenic purpura. Haematologica 95: 1555–1562.
25. Soejima K, Matsumoto M, Kokame K, Yagi H, Ishizashi H, et al. (2003) ADAMTS-13 cysteine-rich/spacer domains are functionally essential for von Willebrand factor cleavage. Blood 102: 3232–3237.
26. Keller KE, Aga M, Bradley JM, Kelley MJ, Acott TS (2009) Extracellular matrix turnover and outflow resistance. Exp Eye Res 88: 676–682.
27. Keller KE, Bradley JM, Acott TS (2009) Differential effects of ADAMTS-1, -4, and -5 in the trabecular meshwork. Invest Ophthalmol Vis Sci 50: 5769–5777.
28. Dagoneau N, Benoist-Lasselin C, Huber C, Faivre L, Megarbane A, et al. (2004) ADAMTS10 mutations in autosomal recessive Weill-Marchesani syndrome. Am J Hum Genet 75: 801–806.
29. Morales J, Al-Sharif L, Khalil DS, Shinwari JM, Bavi P, et al. (2009) Homozygous mutations in ADAMTS10 and ADAMTS17 cause lenticular myopia, ectopia lentis, glaucoma, spherophakia, and short stature. Am J Hum Genet 85: 558–568.
30. Faivre L, Gorlin RJ, Wirtz MK, Godfrey M, Dagoneau N, et al. (2003) In frame fibrillin-1 gene deletion in autosomal dominant Weill-Marchesani syndrome. J Med Genet 40: 34–36.
31. Faivre L, Dollfus H, Lyonnet S, Alembik Y, Megarbane A, et al. (2003) Clinical homogeneity and genetic heterogeneity in Weill-Marchesani syndrome. Am J Med Genet A 123A: 204–207.
32. Ramirez F, Sakai LY (2009) Biogenesis and function of fibrillin assemblies. Cell Tissue Res 339: 71–82.
33. Izquierdo NJ, Traboulsi EI, Enger C, Maumenee IH (1992) Glaucoma in the Marfan syndrome. Trans Am Ophthalmol Soc 90: 111–117; discussion 118–122.
34. Dureau P (2008) Pathophysiology of zonular diseases. Curr Opin Ophthalmol 19: 27–30.
35. Ahram D, Sato TS, Kohilan A, Tayeh M, Chen S, et al. (2009) A homozygous mutation in ADAMTSL4 causes autosomal-recessive isolated ectopia lentis. Am J Hum Genet 84: 274–278.
36. Tektas OY, Lutjen-Drecoll E (2009) Structural changes of the trabecular meshwork in different kinds of glaucoma. Exp Eye Res 88: 769–775.
37. Samuelson DA, Gum GG, Gelatt KN (1989) Ultrastructural changes in the aqueous outflow apparatus of beagles with inherited glaucoma. Invest Ophthalmol Vis Sci 30: 550–561.
38. Tripathi RC, Li J, Chan WF, Tripathi BJ (1994) Aqueous humor in glaucomatous eyes contains an increased level of TGF-beta 2. Exp Eye Res 59: 723–727.
39. Tamm ER, Fuchshofer R (2007) What increases outflow resistance in primary open-angle glaucoma? Surv Ophthalmol 52(Suppl 2): S101–104.
40. Ali M, McKibbin M, Booth A, Parry DA, Jain P, et al. (2009) Null mutations in LTBP2 cause primary congenital glaucoma. Am J Hum Genet 84: 664–671.
41. Silberstein M, Tzemach A, Dovgolevsky N, Fishelson M, Schuster A, et al. (2006) Online system for faster multipoint linkage analysis via parallel execution on thousands of personal computers. Am J Hum Genet 78: 922–935.
42. Abecasis GR, Cherny SS, Cookson WO, Cardon LR (2001) GRR: graphical representation of relationship errors. Bioinformatics 17: 742–743.
43. Albert TJ, Molla MN, Muzny DM, Nazareth L, Wheeler D, et al. (2007) Direct selection of human genomic loci by microarray hybridization. Nat Methods 4: 903–905.
44. Okou DT, Steinberg KM, Middle C, Cutler DJ, Albert TJ, et al. (2007) Microarray-based genomic selection for high-throughput resequencing. Nat Methods 4: 907–909.
45. Langmead B, Trapnell C, Pop M, Salzberg SL (2009) Ultrafast and memory-efficient alignment of short DNA sequences to the human genome. Genome Biol 10: R25.
46. Li H, Handsaker B, Wysoker A, Fennell T, Ruan J, et al. (2009) The Sequence Alignment/Map format and SAMtools. Bioinformatics 25: 2078–2079.
47. Roy A, Kucukural A, Zhang Y (2010) I-TASSER: a unified platform for automated protein structure and function prediction. Nat Protoc 5: 725–738.
48. Jones TA, Zou JY, Cowan SW, Kjeldgaard M (1991) Improved methods for building protein models in electron density maps and the location of errors in these models. Acta Crystallogr A 47(Pt 2): 110–119.
49. Kraulis PJ (1991) Molscript - a Program to Produce Both Detailed and Schematic Plots of Protein Structures. Journal of Applied Crystallography 24: 946–950.
50. Merritt EA, Bacon DJ (1997) Raster3D: photorealistic molecular graphics. Methods Enzymol 277: 505–524.